Polyhedron 224 (2022) 116005

Contents lists available at ScienceDirect

Polyhedron

journal homepage: www.elsevier.com/locate/poly

Versatility within (4,4) networks assembled from 1,4-bis(*n*-alkyloxy)-2,5-bis(3,2′:6′,3′′-terpyridin-4′-yl)benzene and [Cu(hfacac)$_2$] (Hhfacac = 1,1,1,5,5,5-hexafluoropentane-2,4-dione)

Simona S. Capomolla, Giacomo Manfroni, Alessandro Prescimone, Edwin C. Constable, Catherine E. Housecroft *

Department of Chemistry, University of Basel, Mattenstrasse 24a, BPR 1096, 4058 Basel, Switzerland

ARTICLE INFO

We dedicate this manuscript to Arnold (Arnie) Rheingold whose commitment to inorganic crystallography has had a lasting impact on the field. One of us is indebted to Arnie for bringing to life so many organometallic clusters at the start of her academic career.

Keywords:
3,2′:6′,3″-Terpyridine
Copper(II)
Coordination networks
Lattice solvents
X-ray

ABSTRACT

The reactions of 1,4-bis(*n*-alkyloxy)-2,5-bis(3,2′:6′,3′′-terpyridin-4′-yl)benzene ligands with methoxy (**1**), ethoxy (**2**), *n*-propoxy (**3**), *n*-butyloxy (**4**), *n*-pentyloxy (**5**), *n*-hexyloxy (**6**), *n*-heptyloxy (**7**) and *n*-octyloxy (**8**) substituents with [Cu(hfacac)$_2$]·H$_2$O (Hhfacac = 1,1,1,5,5,5-hexafluoropentane-2,4-dione) under conditions of crystal growth by layering have been investigated using different combinations of solvents. The products have been structurally characterized and in all cases, Cu(II) is octahedrally sited in a *trans*-{Cu(hfacac)$_2$(N)$_2$} environment in which N is a pyridine donor in one of the outer rings of a 3,2′:6′,3′′-tpy unit. The coordination assemblies fall into four categories. The most populated class consists of (4,4) nets in which each bis(3,2′:6′,3′′-tpy) ligand **1** and **4–8** acts as a 4-connecting node and the Cu(II) centres lie within the plane defined by the nodes; changes in conformation of the 3,2′:6′,3′′-tpy units do not affect the assembly of the (4,4) network. One of two assemblies isolated with ligand **2** is also a (4,4) net, but powder X-ray diffraction (PXRD) data indicate that this is not representative of the bulk material. [Cu$_2$(hfacac)$_4$(**3**)]$_n$·5.5*n*C$_6$H$_5$Cl exhibits a unique structure consisting of a (4,4) net with the Cu(II) centres lying above and below the plane of the net. A third class of assembly was found for [Cu$_3$(hfacac)$_6$(**5**)$_2$]$_n$ and comprises a (4,4) net in which half of the ligands are 4-connecting nodes and half coordinate through two pyridine rings and are therefore linkers; the efficient packing in this structure leaves no solvent-accessible voids. A 1D-coordination polymer in which all the bis(3,2′:6′,3′′-tpy) ligands are 2-connecting linkers was observed for [Cu$_2$(hfacac)$_4$(**2**)$_2$]$_n$·1.5*n*CHCl$_3$·4*n*MeOH and PXRD data confirm that the structure is representative of the bulk material. Structural studies have been complemented by thermogravimetic analyses of selected compounds.

1. Introduction

Over the past few years, we have been developing the coordination chemistry of 3,2′:6′,3″-terpyridine (3,2′:6′,3″-tpy) ligands with a recent focus on those containing two or three 3,2′:6′,3″-tpy units [1–5]. In contrast to the more popular 2,2′:6′,2″-terpyridine which is typically a bis(chelating) ligand (2,2′:6′,2″-tpy, Scheme 1), 3,2′:6′,3″-tpy coordinates only through the outer pyridine *N*-atoms making it a divergent, rather than convergent, metal-binding domain. Note that there are numerous examples of 2,2′:6′,2″-tpy acting as a hypodentate ligand [6]. Moreover, rotation about the inter-ring C-C bonds in 3,2′:6′,3″-tpy leads to three limiting planar conformations of the unit as shown in Scheme 1. Conformations **I** and **II** are more commonly observed than conformation **III** for which there are relatively few examples [7–16].

Yoshida *et al.* were the first to report a bis(3,2′:6′,3″-tpy) ligand as a 4-connecting node for the assembly of a 2D-network. Reaction of [Co(acacCN)$_2$] (HacacCN = 3-cyanopentane-2,4-dione) with the ligand **L** shown in Scheme 2 led to assembly of [Co$_2$(acacCN)$_4$(**L**)]$_n$ with each 3,2′:6′,3″-tpy unit adopting conformation **II**. Significantly, Yoshida *et al.* also demonstrated that when **L** reacted with [Co(acacPh$_2$)$_2$] (HacacPh$_2$

* Corresponding author.
E-mail address: catherine.housecroft@unibas.ch (C.E. Housecroft).

https://doi.org/10.1016/j.poly.2022.116005
Received 13 May 2022; Accepted 24 June 2022
Available online 29 June 2022

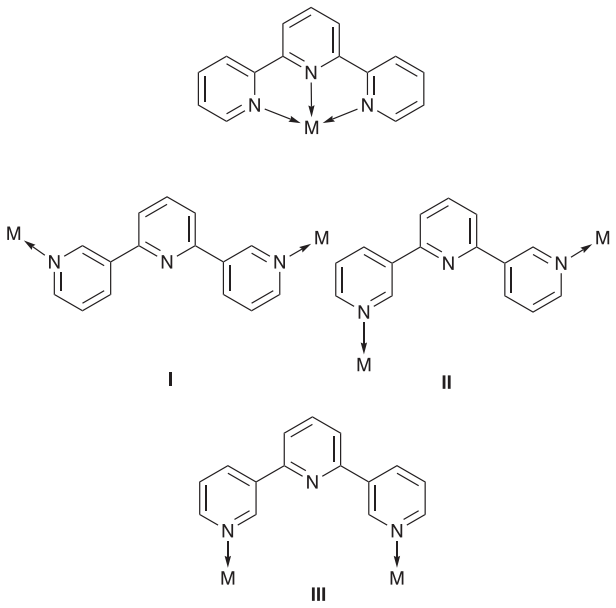

Scheme 1. Top: 2,2′:6′,2″-tpy as a bischelating ligand. Bottom: Limiting planar conformations **I–III** of 3,2′:6′,3″-tpy and metal-binding sites.

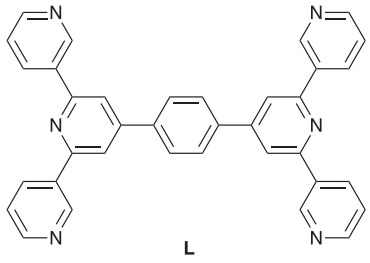

Scheme 2. The bis(3,2′:6′,3″-tpy) ligand **L** reported by Yoshida *et al.* [17].

= 1,3-diphenylpropane-1,3-dione), the steric hindrance of the phenyl substituents directed the assembly to a 1D-coordination polymer [Co(acacPh$_2$)$_2$(**L**)]$_n$ in which **L** behaved only as a ditopic ligand, leaving one outer pyridine ring in each 3,2′:6′,3″-tpy unit uncoordinated [17]. The {Cu(acac)$_2$} and {Cu(hfacac)$_2$} units (Hacac = pentane-2,4-dione, Hhfacac = 1,1,1,5,5,5-hexafluoropentane-2,4-dione) are complementary to {Co(acacPh$_2$)$_2$} and {Co(acacCN)$_2$}, and both copper(II) motifs are well represented in the Cambridge Structural Database (CSD) [18], with coordination assemblies incorporating {Cu(hfacac)$_2$} being more numerous than those containing {Cu(acac)$_2$} motifs. We have suggested that a factor contributing to the dominance of {Cu(hfacac)$_2$}-containing assemblies may be that the CF$_3$ substituents enhance the solubility of the copper(II) salt in a greater variety of solvents than with [Cu(acac)$_2$] [19]. For structures containing octahedral {Cu(hfacac)$_2$(N)$_2$} (N = *N*-donor ligand) units, a *trans*-arrangement of the *N*-donors is usual [3], unless the two *N* donors belong to a chelating ligand.

We now present a systematic investigation of reactions between a series of 1,4-bis(*n*-alkyloxy)-2,5-bis(3,2′:6′,3′′-terpyridin-4′-yl)benzene ligands and [Cu(hfacac)$_2$]. The bis(3,2′:6′,3″-tpy) ligands are related to Yoshida's ligand shown in Scheme 2, with the introduction of two alkyloxy substituents ranging in length from methoxy to *n*-octyloxy. In addition to improving ligand solubility, we were motivated to discover how the coordination assembly was influenced by the differing steric demands of the alkyloxy chains. Crystals of the coordination assemblies were grown under ambient conditions using a solvent-layering technique (see Supplementary Materials for details) and we address the effects that different solvents have on the solid-state structures.

2. Materials and methods

2.1. General

^{1}H and ^{13}C{^{1}H} spectra were recorded on a Bruker Avance III-500 spectrometer equipped with a BBFO probehead at 298 K. The ^{1}H and ^{13}C NMR chemical shifts were referenced with respect to residual solvent peaks (δ 7.26 ppm for $CHCl_3$ and δ 77.2 ppm for $CDCl_3$, respectively with δ TMS = 0). Matrix-assisted laser desorption ionization time-of-flight (MALDI-TOF) mass spectra were recorded on a Shimadzu MALDI 8020 instrument without matrix. PerkinElmer UATR Two and Shimadzu UV-2600 instruments were used to record FT-IR and UV-vis absorption spectra, respectively. Melting points were determined using a Stuart melting point SMP 30 device. Elemental analyses and high-resolution electrospray (HR-ESI) mass spectra were performed using a Vario MICRO Cube device and Bruker maXis 4G QTOF instrument, respectively.

Thermogravimetric analyses (TGA) were performed on a TGA5500 instrument coupled to a Discovery II MS, Cirrus 3 mass spectrometer. The analyses were carried under nitrogen, using a Barchart scanning method in the mass range 10–125 or 12–160 in the case of 1,2-dichlorobenzene. In all experiments, the temperature of the TGA instrument was initially stabilized at 30 °C. The samples were heated to 170 °C (210 °C if 1,2-dichlorobenzene was involved) and this temperature was maintained for 30 min. During this time, it was possible to detect the solvent being released from the coordination network (see text) and solvents were identified using mass spectrometry.

Analytical thin-layer chromatography was conducted with pre-coated silica gel 60 F_{254} aluminium sheets (Merck KGaA) and visualized using UV light (254 nm and 366 nm). Flash column chromatography was performed on a Biotage Selekt system with pre-packed silica gel columns (50 g Biotage Sfär Silica High Capacity Duo 20 μm) using ethyl acetate in cyclohexane (gradient) as eluent and monitoring and collecting at 366 nm.

3-Acetylpyridine, 1-bromopropane, 1-bromobutane and 1-bromoheptane were purchased from Acros Organics and 1-bromoethane, and 1-bromohexane were from Alfa Aesar. 1-Bromopentane, 1-bromooctane and 2,5-dimethoxybenzene-1,4-dicarbaldehyde were bought from Sigma-Aldrich, and 2,5-dibromobenzene-1,4-diol from Fluorochem. [Cu(hfacac)$_2$]·H_2O was purchased from abcr GmbH. All chemicals were used as received.

All crystal growth experiments were carried out under ambient conditions using glass test-tubes (i.d. = 13.6 mm, 24 mL).

2.2. Ligand syntheses

Synthetic procedures for the synthesis of ligands **1–7** are given in the Supplementary Materials, along with characterization data. Ligand **8** was prepared according to a previously reported method [1].

2.3. Crystallography

Single crystal data were collected on a STOE StadiVari Eulerian 4-circle diffractometer (CuKα radiation) equipped with a Dectris Eiger2 1 M detector, or using a STOE StadiVari diffractometer equipped with a Pilatus300K detector and with a Metaljet D2 source (GaKα radiation) with data processing using STOE software (X-Area 1.90, STOE, 2020). Structures were solved using Superflip [20,21] and Olex2 [22]. The model was refined with ShelXL v. 2018/3 [23]. See the Supplementary Materials for the radiation type (Cu or Ga) for each structure. All H atoms were included at geometrically calculated positions and refined using a riding model with U_{iso} = 1.2 of the parent atom. Structure analysis and structural diagrams used CSD Mercury 2021.3.0 [24]. Crystallographic data for all compounds are given in the Supplementary Materials.

In most structures, one or more of the CF$_3$ groups was rotationally

disordered, and the longer alkyloxy chains also suffered from disorder. Details of the treatment of the disorders and site occupancies are given in the Supplementary Materials in the relevant figure captions. $[Cu_2(hfacac)_4(\mathbf{2})_2]_n{\cdot}1.5n CHCl_3{\cdot}4n MeOH$ was refined as a two-component inversion twin. The solvent molecules in all the structures with solvate were disordered. In $[Cu_2(hfacac)_4(\mathbf{5})]_n{\cdot}3.5n C_6H_4Cl_2$, geometrical restraints for the aromatic ring and restraints for the thermal parameters had to be used to treat the $C_6H_4Cl_2$ molecules. A solvent mask was applied to part or all the solvent region in $[Cu_2(hfacac)_4(\mathbf{1})]_n{\cdot}3n CHCl_3$, $[Cu_2(hfacac)_4(\mathbf{2})]_n{\cdot}1.2n CHCl_3$, $[Cu_2(hfacac)_4(\mathbf{3})]_n{\cdot}5.5n C_6H_5Cl$, $[Cu_2(hfacac)_4(\mathbf{4})]_n{\cdot}4n MeC_6H_5$, $[Cu_2(hfacac)_4(\mathbf{4})]_n{\cdot}3.5n C_6H_4Cl_2$, $[Cu_2(hfacac)_4(\mathbf{6})]_n{\cdot}2.4n MeC_6H_5$, $[Cu_2(hfacac)_4(\mathbf{7})]_n{\cdot}2.4n CHCl_3$, $[Cu_2(hfacac)_4(\mathbf{7})]_n{\cdot}2.6n CHCl_3$ (both polymorphs), $[Cu_2(hfacac)_4(\mathbf{7})]_n{\cdot}2n MeC_6H_5$, and $[Cu_2(hfacac)_4(\mathbf{8})]_n{\cdot}1.6n CHCl_3$. In each case, the electron density removed was accounted for in terms of added solvent molecules and these were added to the formulae and all appropriate numbers.

Powder X-ray diffraction (PXRD) data were collected at room temperature (ca. 295 K) in transmission mode using a Stoe Stadi P diffractometer equipped with CuKα1 radiation (Ge(1 1 1)) monochromator and a DECTRIS MYTHEN 1 K detector.

3. Results and discussion

3.1. Ligand syntheses and crystal structure of dialdehyde 6b

Ligand **1** was prepared from the commercially available 2,5-dimethoxybenzene-1,4-dicarbaldehyde according to Scheme 3, and ligand **8** was prepared as previously reported [1]. The strategy shown in Scheme 4 was used to synthesize compounds **2–7**. While other routes have been described in the literature to access 1,4-dibromo-2,5-bis(alkyloxy)benzene intermediates (for example, bromination of hydroquinone diethers [25]), the route we selected via the commercially available 2,5-dibromobenzene-1,4-diol proved to be very efficient. The functionalization of 2,5-dibromobenzene-1,4-diol with an alkyl bromide was carried out under basic conditions with yields in the range 62–89 % for compounds **2a–7a** (Scheme 4). Compounds **2b–7b** (Scheme 4) were prepared using a Bouveault aldehyde synthesis [26] with *n*-BuLi and DMF. The dialdehydes were converted to the bis(3,2′:6′,3″-tpy) ligands **2–7** by reaction with 3-acetylpyridine using the one-pot strategy of Hanan [27]. Full synthetic details for the intermediates and final products shown in Schemes 3 and 4 are provided in the Supplementary Materials. The ^1H and $^{13}C\{^1H\}$ NMR spectra of **2a–7a** and **2b–7b** are shown in Figs. S1–S24.

Single crystals of dialdehyde **6b** grew from a hot petroleum ether solution of the compound as it was allowed to cool to room temperature (ca. 22 °C). The compound crystallizes in the triclinic space group *P*–1, and the asymmetric unit comprises two independent half-molecules

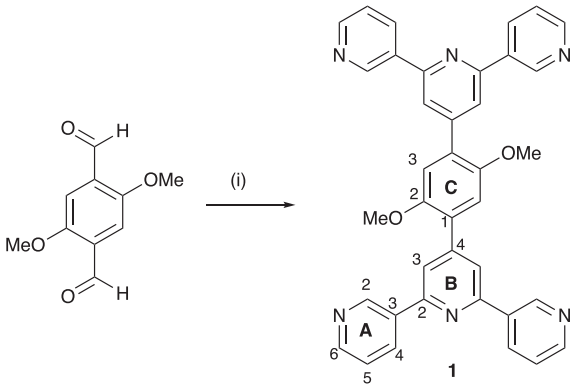

Scheme 3. Synthesis of ligand **1**. Conditions: (i) 3-acetylpyridine, KOH, EtOH, aqueous NH_3, room temperature.

with each arene-centroid lying on an inversion centre. The structure of one of the independent molecules of **6b** is shown in Fig. 1; both molecules are structurally similar with the *n*-hexyloxy chains in extended conformations. Crystal packing is dominated by intermolecular O…H—C hydrogen bonds.

3.2. Characterization of ligands 1–7

Ligands **1–7** were characterized by ^1H and $^{13}C\{^1H\}$ NMR, solid-state FT-IR and solution absorption spectroscopies, as well as MALDI-TOF mass spectrometry, and either elemental analysis or high-resolution electrospray (HR-ESI) mass spectrometry. In the MALDI-TOF mass spectrum of each compound, the base peak corresponded to the $[M + H]^+$ ion as shown in Figs. S25–S31. Where elemental analytical results were not within acceptable limits, a high-resolution electrospray mass spectrum was also recorded (Figs. S32–S35). The ^1H and $^{13}C\{^1H\}$ NMR spectra were assigned using 2D methods (COSY, NOESY, HMQC and HMBC spectra) and were in accord with the structures shown in Scheme 3 and 4. Figures S36 to S63 display the ^1H NMR, $^{13}C\{^1H\}$ NMR, HMQC and HMBC spectra of each of compounds **1–7**, and full assignments are provided in the experimental sections in the Supplementary Materials. Fig. 2 illustrates that the length of the alkyloxy substituent has little effect on the aromatic regions of the ^1H NMR spectra of **1–7** except in the case of the OMe group, when signal for the H^{B3} (the aromatic proton on the central pyridine ring, Scheme 3) was shifted to lower frequency (δ 8.00 ppm in **1** compared to δ 8.03 or 8.04 ppm in **2–7**).

Fig. 3 displays the solution absorption spectra of compounds **1–7**. The spectra exhibit similar absorption bands arising from spin-allowed $\pi^*\leftarrow\pi$ transitions. The length of the *n*-alkyloxy chain on the phenylene spacer of the bis(3,2′:6′,3″-tpy) ligands does not significantly influence the absorption spectra. The values of λ^{max} = 277 (shoulder), 315 and 353 nm for **1** are characteristic of all the ligands, and of the previously reported *n*-octyloxy derivative **8** [1]. The solid-state IR spectra of **1–7** (Figs. S64–S70) show characteristic absorptions in the fingerprint region and peaks around 3000 cm^{-1} arising from aliphatic C-H stretches which increase in relative intensity as the length of the alkyloxy substituents increases.

3.3. Crystal growth experiments

Reactions between each of ligands **1–8** and $[Cu(hfacac)_2]{\cdot}H_2O$ were carried out under conditions of crystallization by layering at room temperature (ca. 22 °C). In addition to probing the effects of the different alkyloxy substituents on solid-state structure, we were also interested in the effects of solvent. Table 1 summarizes the solvent combinations from which X-ray quality crystals were obtained; full details of crystal growth conditions are given in the Supplementary Materials. Many of the crystals were sensitive to loss of solvent and this can be rationalized in terms of the porosity of the structures described below.

Single crystals grew from more than one solvent combination in the case of the ligands **4**, **5** and **7** and X-ray diffraction data were collected for all crystals. For the combination of **5** and $[Cu(hfacac)_2]{\cdot}H_2O$, crystals of $[Cu_3(hfacac)_6(\mathbf{5})_2]_n$ were obtained from two solvent combinations (Table 1) and the space group ($P2_1/c$) and cell parameters (a = 11.9727 (2) Å, b = 37.6012(4) Å, c = 14.5251(2) Å, β = 102.3690(10)° for crystals grown from MeOH and toluene; a = 11.96060(10) Å, b = 37.6107(5) Å, c = 14.5313(2) Å, β = 102.3980(10)° for crystals grown from MeOH and $CHCl_3$) were consistent with a common structure. Only that for crystals from MeOH and toluene is discussed in detail below. Note that the coordination network in $[Cu_2(hfacac)_4(\mathbf{5})]_n{\cdot}3.5n C_6H_4Cl_2$ (Table 1) differs from $[Cu_3(hfacac)_6(\mathbf{5})_2]_n$ and is discussed separately. Reactions between **7** and $[Cu(hfacac)_2]{\cdot}H_2O$ using four different solvent combinations (Table 1) produced X-ray quality crystals of $[Cu_2(hfacac)_4(\mathbf{7})]_n{\cdot}2.4n CHCl_3$ (from MeOH/$CHCl_3$), $[Cu_2(hfacac)_4(\mathbf{7})]_n{\cdot}2.6n CHCl_3$ (polymorph A, from EtOH/$CHCl_3$), $[Cu_2(hfacac)_4(\mathbf{7})]_n{\cdot}2.6n CHCl_3$

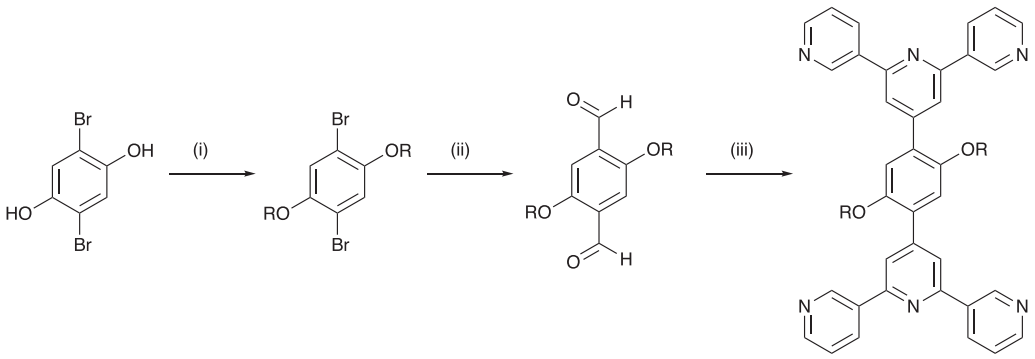

2a R = Ethyl
3a R = ^{n}Propyl
4a R = ^{n}Butyl
5a R = ^{n}Pentyl
6a R = ^{n}Hexyl
7a R = ^{n}Heptyl

2b R = Ethyl
3b R = ^{n}Propyl
4b R = ^{n}Butyl
5b R = ^{n}Pentyl
6b R = ^{n}Hexyl
7b R = ^{n}Heptyl

2 R = Ethyl
3 R = ^{n}Propyl
4 R = ^{n}Butyl
5 R = ^{n}Pentyl
6 R = ^{n}Hexyl
7 R = ^{n}Heptyl

Scheme 4. Synthesis of ligands **2**–**7**. Conditions: (i) RBr, anhydrous K_2CO_3, dry DMF, 100 °C; (ii) ^{n}BuLi, dry Et_2O, 0 °C; dry DMF, 0 °C warmed to room temperature; (iii) 3-acetylpyridine, KOH, EtOH, aqueous NH_3, room temperature.

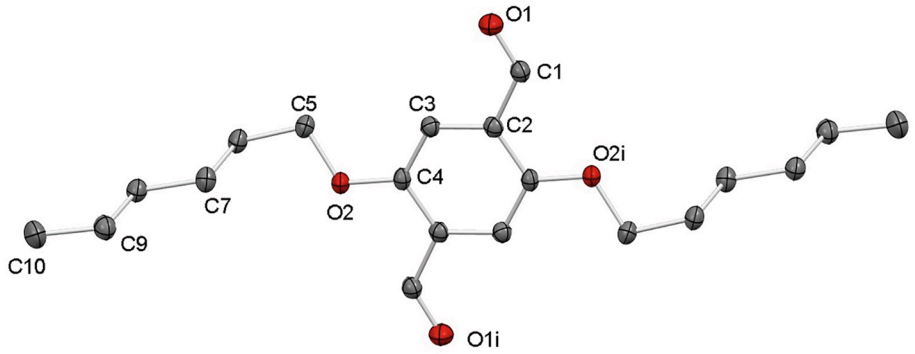

Fig. 1. Structure of one of the two independent molecules of **6b** with H atoms omitted for clarity; ellipsoids are plotted at a 40 % probability level. Symmetry code i = 1–*x*, 1–*y*, 1–*z*. Selected bond parameters: C1–O1 = 1.2098(15), C1–*C*2 = 1.4771(17), O2–C4 = 1.3634(14), O2–C5 = 1.4400(14) Å; C4–O2–C5 = 116.79(9)°.

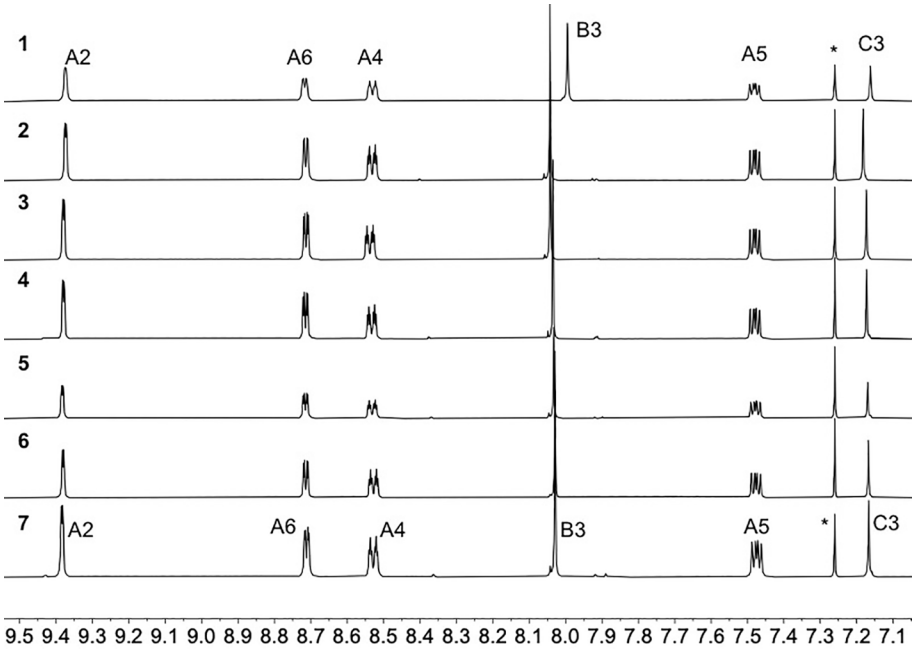

Fig. 2. The aromatic regions of the ^{1}H NMR spectra of compounds **1**–**7** (500 MHz, $CDCl_3$, 298 K). Scale in δ/ppm. * = residual $CHCl_3$.

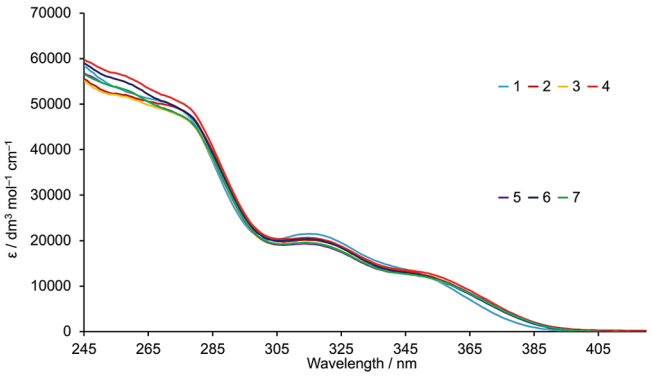

Fig. 3. Solution absorption spectra ($CHCl_3$, 2.0 × 10^{-5} mol/dm^{-3}) of ligands **1**–**7**.

(polymorph B, from ^{t}BuOH/$CHCl_3$) and $[Cu_2(hfacac)_4(\mathbf{7})]_n{\cdot}2n MeC_6H_5$ (from MeOH/ toluene). All crystallized in the triclinic space group *P*–1, and an overlay of the repeating units (Fig. 4) showed the ligand conformations and connectivities to be virtually identical, and propagation into a 2D-network (see below) was also the same. The crystal structure of $[Cu_2(hfacac)_4(\mathbf{7})]_n{\cdot}2.6nCHCl_3$ (polymorph B) obtained from ^{t}BuOH/$CHCl_3$ will be described in detail as being representative of the four networks. In the case of $[Cu(hfacac)_2]{\cdot}H_2O$ and ligand **4**, single crystals of $[Cu_2(hfacac)_4(\mathbf{4})]_n{\cdot}3.5nC_6H_4Cl_2$ and $[Cu_2(hfacac)_4(\mathbf{4})]_n{\cdot}4nMeC_6H_5$ (Table 1) were obtained and the differences in network assembly warrant separate discussion of these structures. For ligands **1**, **2**, **3**, **6** and **8** good quality single crystals were obtained only for the solvent combinations given in Table 1.

Overall, fifteen crystal structures were determined and these fall into four structural groups: (4,4) nets directed by the 4-connecting ligand nodes with Cu(II) centres lying in the plane of the net, a (4,4) net with Cu (II) centres lying above and below the plane of the net, a (4,4) net in which half of the ligands are 4-connecting nodes and half are linkers, and a 1D-coordination polymer in which each ligand coordinates through only two *N*-donors. Each structure-type is discussed in detail below.

3.4. Bis(3,2′:6′,3″-tpy) ligands as 4-connecting nodes: Assembly of (4,4) nets

Each of $[Cu_2(hfacac)_4(\mathbf{1})]_n{\cdot}3nCHCl_3$, $[Cu_2(hfacac)_4(\mathbf{2})]_n{\cdot}1.2nCHCl_3$, $[Cu_2(hfacac)_4(\mathbf{4})]_n{\cdot}3.5nC_6H_4Cl_2$, $[Cu_2(hfacac)_4(\mathbf{4})]_n{\cdot}4nMeC_6H_5$, $[Cu_2(hfacac)_4(\mathbf{5})]_n{\cdot}3.5nC_6H_4Cl_2$, $[Cu_2(hfacac)_4(\mathbf{6})]_n{\cdot}2.4nMeC_6H_5$, $[Cu_2(hfacac)_4(\mathbf{7})]_n{\cdot}2.6nCHCl_3$ (polymorph B, see Section 3.2) and $[Cu_2(hfacac)_4(\mathbf{8})]_n{\cdot}1.6nCHCl_3$ crystallizes in the triclinic space group *P*–1 and the structures of the asymmetric units are shown in Figs. S71–S78. Each bis (3,2′:6′,3″-tpy) ligand acts as a 4-connecting node with each outer pyridine ring coordinating to one Cu atom of a different $\{Cu(hfacac)_2\}$ unit, and the structures propagate into 2-dimensional (4,4)-nets. Each Cu atom has a *trans*-arrangement of pyridine donors, and the Cu–N and Cu–O bond lengths are unexceptional (Table 2). In $[Cu_2(hfacac)_4(\mathbf{1})]_n{\cdot}3nCHCl_3$, $[Cu_2(hfacac)_4(\mathbf{2})]_n{\cdot}1.2nCHCl_3$, $[Cu_2(hfacac)_4(\mathbf{5})]_n{\cdot}3.5nC_6H_4Cl_2$ and $[Cu_2(hfacac)_4(\mathbf{8})]_n{\cdot}1.6nCHCl_3$, the 3,2′:6′,3″-tpy domain in each of ligands **1**, **2**, **5** and **8** adopts conformation **II** (Scheme 1), while in $[Cu_2(hfacac)_4(\mathbf{4})]_n{\cdot}3.5nC_6H_4Cl_2$, $[Cu_2(hfacac)_4(\mathbf{4})]_n{\cdot}4nMeC_6H_5$, $[Cu_2(hfacac)_4(\mathbf{6})]_n{\cdot}2.4nMeC_6H_5$ and $[Cu_2(hfacac)_4(\mathbf{7})]_n{\cdot}2.6nCHCl_3$, all 3,2′:6′,3″-tpy units in ligands **4**, **6** and **7** adopt conformation **I** (Scheme 1). However, the change in conformation does not affect the ability of the ligand to direct the assembly into a (4,4) network. Table 3 summarizes how the ligand conformation varies throughout the series, and the network is exemplified for $[Cu_2(hfacac)_4(\mathbf{1})]_n{\cdot}3nCHCl_3$ in Fig. 5. In all the structures in this series, the Cu atoms lie in or close to the plane through the 4-connecting nodes that define the (4,4)-net. Fig. 6 shows a view into this plane in $[Cu_2(hfacac)_4(\mathbf{1})]_n{\cdot}3nCHCl_3$ and

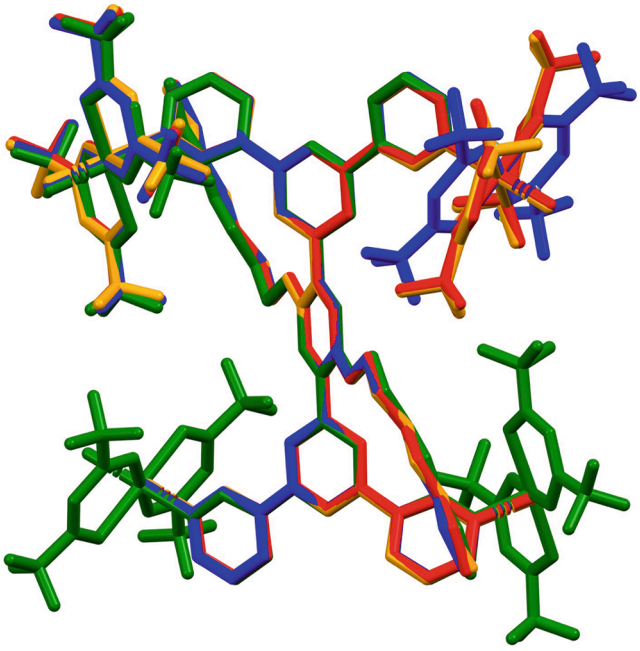

Fig. 4. Overlay of the repeating units in $[Cu_2(hfacac)_4(\mathbf{7})]_n{\cdot}2.4nCHCl_3$ (blue), $[Cu_2(hfacac)_4(\mathbf{7})]_n{\cdot}2.6nCHCl_3$ (polymorph A, red), $[Cu_2(hfacac)_4(\mathbf{7})]_n{\cdot}2.6nCHCl_3$ (polymorph B, orange), and $[Cu_2(hfacac)_4(\mathbf{7})]_n{\cdot}2nMeC_6H_5$ (green). (Colour online.)

Table 1
Crystalline products and solvents used for the layering experiments, and space groups; cell parameters are given in the Supplementary Materials.

Compound	Solvent for $[Cu(hfacac)_2]{\cdot}H_2O$	Solvent for ligand	Space group
$[Cu_2(hfacac)_4(\mathbf{1})]_n{\cdot}3nCHCl_3$	EtOH	$CHCl_3$	*P*–1
$[Cu_2(hfacac)_4(\mathbf{2})_2]_n{\cdot}1.5nCHCl_3{\cdot}4n$MeOH	MeOH	$CHCl_3$	$Pca2_1$
$[Cu_2(hfacac)_4(\mathbf{2})]_n{\cdot}1.2nCHCl_3$	MeOH	$CHCl_3$	*P*–1
$[Cu_2(hfacac)_4(\mathbf{3})]_n{\cdot}5.5nC_6H_5Cl$	Chlorobenzene	$CHCl_3$	*P*–1
$[Cu_2(hfacac)_4(\mathbf{4})]_n{\cdot}3.5nC_6H_4Cl_2$	MeOH	1,2-Dichlorobenzene	*P*–1
$[Cu_2(hfacac)_4(\mathbf{4})]_n{\cdot}4nMeC_6H_5$	MeOH	Toluene	*P*–1
$[Cu_3(hfacac)_6(\mathbf{5})_2]_n$	MeOH	Toluene	$P2_1/c$
$[Cu_3(hfacac)_6(\mathbf{5})_2]_n$	MeOH	$CHCl_3$	$P2_1/c$
$[Cu_2(hfacac)_4(\mathbf{5})]_n{\cdot}3.5nC_6H_4Cl_2$	MeOH	1,2-Dichlorobenzene	*P*–1
$[Cu_2(hfacac)_4(\mathbf{6})]_n{\cdot}2.4nMeC_6H_5$	MeOH	Toluene	*P*–1
$[Cu_2(hfacac)_4(\mathbf{7})]_n{\cdot}2.4nCHCl_3$	MeOH	$CHCl_3$	*P*–1
$[Cu_2(hfacac)_4(\mathbf{7})]_n{\cdot}2.6nCHCl_3$ (polymorph A)	EtOH	$CHCl_3$	*P*–1
$[Cu_2(hfacac)_4(\mathbf{7})]_n{\cdot}2.6nCHCl_3$ (polymorph B)	^{t}BuOH	$CHCl_3$	*P*–1
$[Cu_2(hfacac)_4(\mathbf{7})]_n{\cdot}2nMeC_6H_5$	MeOH	Toluene	*P*–1
$[Cu_2(hfacac)_4(\mathbf{8})]_n{\cdot}1.6nCHCl_3$	EtOH	$CHCl_3$	*P*–1

Table 2
Cu–O and Cu–N bond lengths in $[Cu_2(hfacac)_4(\mathbf{1})]_n{\cdot}3n CHCl_3$, $[Cu_2(hfacac)_4(\mathbf{2})]_n{\cdot}1.2n CHCl_3$, $[Cu_2(hfacac)_4(\mathbf{4})]_n{\cdot}3.5n C_6H_4Cl_2$, $[Cu_2(hfacac)_4(\mathbf{4})]_n{\cdot}4n MeC_6H_5$, $[Cu_2(hfacac)_4(\mathbf{5})]_n{\cdot}3.5n C_6H_4Cl_2$, $[Cu_2(hfacac)_4(\mathbf{6})]_n{\cdot}2.4n MeC_6H_5$, $[Cu_2(hfacac)_4(\mathbf{7})]_n{\cdot}2.6n CHCl_3$ (polymorph B) and $[Cu_2(hfacac)_4(\mathbf{8})]_n{\cdot}1.6n CHCl_3$.

Compound	Cu–O/Å	Cu–N/Å
$[Cu_2(hfacac)_4(\mathbf{1})]_n{\cdot}3n CHCl_3$	2.229(6), 2.028(7), 2.242 (7), 2.037(7)	2.003(6), 1.998(7)
$[Cu_2(hfacac)_4(\mathbf{2})]_n{\cdot}1.2n CHCl_3$	2.015(6), 2.253(7), 2.333 (6), 2.012(5)	2.017(6), 1.995(7)
$[Cu_2(hfacac)_4(\mathbf{4})]_n{\cdot}3.5n C_6H_4Cl_2$	2.260(3), 1.990(3), 2.058 (3), 2.226(3), 2.040(3), 2.208(3), 2.209(3), 2.053 (3)	1.999(4), 1.981 (4), 2.017(4), 2.010(3)
$[Cu_2(hfacac)_4(\mathbf{4})]_n{\cdot}4n MeC_6H_5$	1.9848(17), 1.9838(17) 2.2747(17), 2.2877(17), 1.9623(17), 1.9637(17), 2.2984(17), 2.2732 (19)	2.022(2), 2.0230 (19), 2.0276(19), 2.0244(19)
$[Cu_2(hfacac)_4(\mathbf{5})]_n{\cdot}3.5n C_6H_4Cl_2$	2.062(5), 2.225(6), 2.308 (4), 1.970(4)	1.998(5), 2.008(5)
$[Cu_2(hfacac)_4(\mathbf{6})]_n{\cdot}2.4n MeC_6H_5$	2.048(4), 2.201(4), 1.983 (4), 2.285(3)	1.992(4), 1.995(3)
$[Cu_2(hfacac)_4(\mathbf{7})]_n{\cdot}2.6n CHCl_3$[a]	2.159(4), 2.091(5), 2.132 (4), 2.142(4)	1.996(5), 2.006(4)
$[Cu_2(hfacac)_4(\mathbf{8})]_n{\cdot}1.6n CHCl_3$	1.968(3), 2.336(3), 1.988 (4), 2.287(4), 2.250(4), 1.994(4), 2.005(4), 2.295 (5)	2.023(3), 2.004 (4),2.001(4), 2.005 (4)

[a] Polymorph B.

Table 3
Conformational differences in the 3,2′:6′,3″-tpy domains in the compounds that form (4,4) networks.

Compound	Conformation[a]	Angle between planes of adjacent py rings/°	Angle between planes of central py and arene rings/°
$[Cu_2(hfacac)_4(\mathbf{1})]_n{\cdot}3n CHCl_3$	**II**	16.0, 17.7	52.1
$[Cu_2(hfacac)_4(\mathbf{2})]_n{\cdot}1.2n CHCl_3$	**II**	8.7, 31.1	33.4
$[Cu_2(hfacac)_4(\mathbf{4})]_n{\cdot}3.5n C_6H_4Cl_2$	**I**	36.1, 38.8[b] 32.1, 40.7[c]	34.3[b] 42.0[c]
$[Cu_2(hfacac)_4(\mathbf{4})]_n{\cdot}4n MeC_6H_5$	**I**	3.8, 30.1[b] 3.8, 29.4[c]	48.2[b] 50.3[c]
$[Cu_2(hfacac)_4(\mathbf{5})]_n{\cdot}3.5n C_6H_4Cl_2$	**II**	2.8, 34.5	40.7
$[Cu_2(hfacac)_4(\mathbf{6})]_n{\cdot}2.4n MeC_6H_5$	**I**	4.8, 37.0	36.8
$[Cu_2(hfacac)_4(\mathbf{7})]_n{\cdot}2.6n CHCl_3$[d]	**I**	4.3, 37.6	39.2
$[Cu_2(hfacac)_4(\mathbf{8})]_n{\cdot}1.6n CHCl_3$	**II**	15.3, 17.6[b] 9.6, 13.5[c]	46.1[b] 45.3[c]

[a] See Scheme 1; [b]for 3,2′:6′,3″-tpy unit containing N2; [c]for 3,2′:6′,3″-tpy unit containing N5; [d]Polymorph B.

$[Cu_2(hfacac)_4(\mathbf{8})]_n{\cdot}1.6n CHCl_3$ with methoxy and octyloxy substituents, respectively. With the exception of the ethoxy substituents, the alkyloxy chains are directed above and below the network and the longest chains are accommodated in cavities in an adjacent sheet.

As previously mentioned, the crystalline samples were sensitive to solvent loss and in the crystal structures, the solvent molecules were disordered to an extent that a solvent mask was used to treat part or all of the solvent regions (see experimental details). Fig. 7 illustrates the solvent-accessible channels in $[Cu_2(hfacac)_4(\mathbf{4})]_n{\cdot}3.5n C_6H_4Cl_2$ and $[Cu_2(hfacac)_4(\mathbf{6})]_n{\cdot}2.4n MeC_6H_5$. For these two compounds, TGA coupled with mass spectrometry was used to verify the identity and amount of solvent in the lattice. The results are summarized in Table 4.

3.5. Structure of $[Cu_2(hfacac)_4(\mathbf{3})]_n{\cdot}5.5n C_6H_5Cl$

$[Cu_2(hfacac)_4(\mathbf{3})]_n{\cdot}5.5n C_6H_5Cl$ crystallizes in the triclinic space group *P*–1. The asymmetric unit (Fig. S79) contains two crystallographically independent half-ligands **3** and two independent copper(II) centers, Cu1 and Cu2; the second half is generated by inversion. Each Cu atom is octahedrally sited with a *trans*-arrangement of *N*-donors. The Cu–N (2.009(5), 1.992(4), 1.987(4) and 2.012(4) Å) and Cu–O bond lengths (range 2.082(6) to 2.188(6) Å) are unexceptional. In both independent ligands, the 3,2′:6′,3″-tpy unit adopts conformation **II** (Scheme 1), and since Cu1 and Cu2 do not lie on inversion centers, there are three possible coordination modes for the *trans*-arrangement of the terpyridine units at each Cu centre (Scheme 5). At both Cu1 and Cu2, the pairs of 3,2′:6′,3″-tpy domains adopt the arrangement shown in Scheme 5c.

Each molecule of coordinated **3** is a 4-connecting node, and the structure propagates into a (4,4) net with close to square shortest-circuits (internal angles 89.7 and 90.3°, Fig. 8a) with the {Cu(hfacac)} linkers lying above and below the plane containing the ligand nodes (Fig. 8b and 8c); the two crystallographically independent ligand nodes are topologically identical. A comparison of Fig. 8b and 6 shows that the positions of the Cu atoms in a sheet in $[Cu_2(hfacac)_4(\mathbf{3})]_n{\cdot}5.5n C_6H_5Cl$ are noticeably different from those in the 2D-networks described in Section 3.3.

Solvent molecules in $[Cu_2(hfacac)_4(\mathbf{3})]_n{\cdot}5.5n C_6H_5Cl$ suffered severe disorder and a solvent mask had to be applied to the solvent region (see experimental section). The solvent-free structure exhibits large voids and channels running along all three crystallographic axes which account for ca. 44 % void space (calculated in Mercury 2021.3.0 [24] using a contact surface map with probe radius = 1.2 Å). As a result, the crystals were highly sensitive to solvent loss.

3.6. Structure of $[Cu_3(hfacac)_6(\mathbf{5})_2]_n$

Of the coordination networks described in this work, $[Cu_3(hfacac)_6(\mathbf{5})_2]_n$ is unique in crystallizing without lattice solvent and in forming an intriguing 2D-network in which half the ligands **5** act as 4-connecting nodes, and half are merely linkers. The compound crystallizes in the monoclinic space group $P2_1/c$, and the asymmetric unit comprises two crystallographically independent half-ligands **5**. There are two independent Cu atoms, and atom Cu1 lies on a special position, giving 1.5 Cu atoms per asymmetric unit. Each of Cu1 and Cu2 is octahedrally sited and is bound by two $[hfacac]^-$ ligands and two pyridine rings of two different ligands **5**, the latter being mutually *trans* (Fig. S80). Each crystallographically independent 3,2′:6′,3″-tpy domain adopts conformation **II** (Scheme 1), although the angles between the pyridine ring planes in each 3,2′:6′,3″-tpy unit are distinct (6.8° and 19.8° for the tpy unit with N1N2N3, and 20.0° and 35.1° for the tpy containing N4N5N6, see Fig. S80 for numbering). The Cu–N (2.028(5), 2.010(5), 2.008(5) Å) and Cu–O (range 2.042(5) to 2.250(5) Å) bond lengths are typical. The two independent ligands exhibit different coordination modes. While that containing N1, N3, N1i and N3i (Fig. 9a) acts as a 4-connecting node, that with N4, N6, N4iii and N6iii (Fig. 9a) coordinates only through N4 and N4iii and is therefore a linker in the coordination assembly (Fig. 9a). The structure propagates into a (4,4) net as shown in Fig. 9b with one dimension of the shortest circuits being approximately doubled compared to those in the (4,4) nets containing ligands **1**, **2**, and **4–8** described above (compare Fig. 9b with Figs. 5 and 8a).

Fig. 10 displays part of one sheet in $[Cu_3(hfacac)_6(\mathbf{5})_2]_n$ viewed down the *b*-axis. The upper and lower faces of the sheets are decorated with CF_3 groups and non-coordinated pyridine rings. In contrast to the non-coordinated pyridine ring found in $[Cu_2(hfacac)_4(\mathbf{2})_2]_n{\cdot}1.5n CHCl_3{\cdot}4n MeOH$ (see next section), non-coordinated N6 (Fig. 9a) shows no short contacts. The pentyloxy chains are in folded conformations and are accommodated within the sheet (Fig. 10). The sheets are efficiently

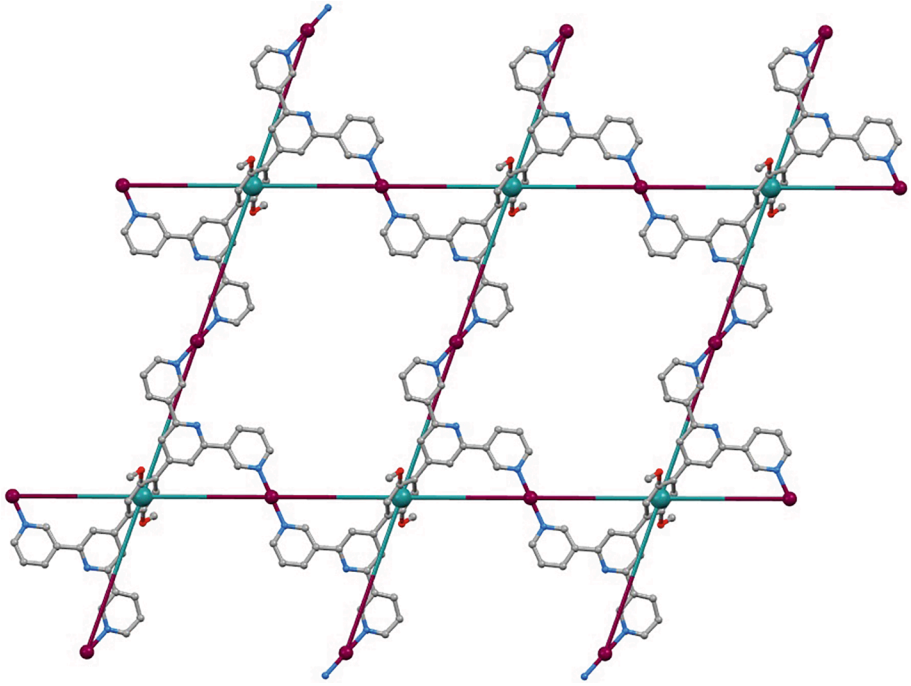

Fig. 5. Part of the (4,4) network in $[Cu_2(hfacac)_4(\mathbf{1})]_n{\cdot}3n CHCl_3$; the 4-connecting node lies at the centre of the arene ring of the ligand and is marked in green. H atoms, $[hfacac]^-$ ligands and solvent molecules are omitted. (Colour online.)

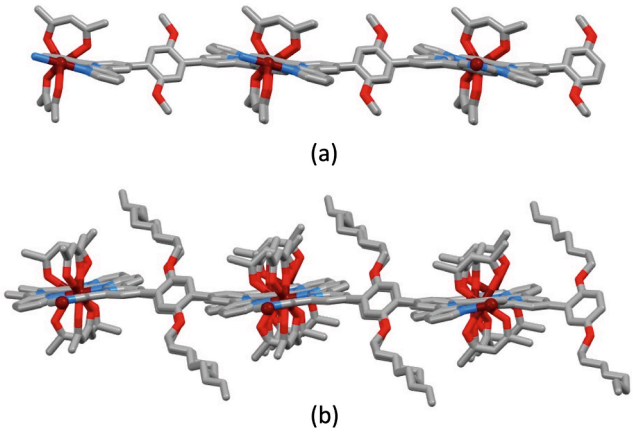

Fig. 6. View into the plane of the (4,4) nets in (a) $[Cu_2(hfacac)_4(\mathbf{1})]_n{\cdot}3n CHCl_3$ and (b) $[Cu_2(hfacac)_4(\mathbf{8})]_n{\cdot}1.6n CHCl_3$. H atoms, F atoms of the $[hfacac]^-$ ligands and solvent molecules are omitted.

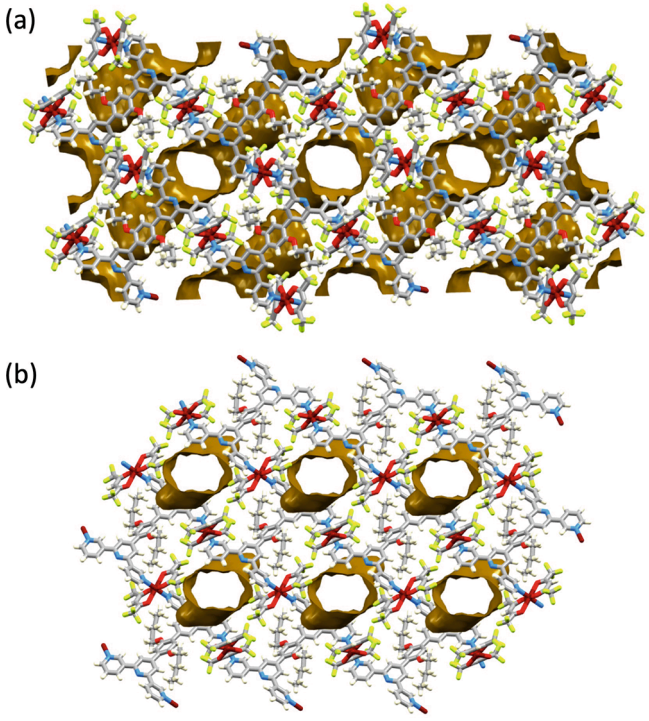

Fig. 7. Representations of the solvent-accessible void space in the crystal lattices of (a) $[Cu_2(hfacac)_4(\mathbf{4})]_n{\cdot}3.5n C_6H_4Cl_2$ (ca. 30 % void) with channels following the *a*-axis, and (b) $[Cu_2(hfacac)_4(\mathbf{6})]_n{\cdot}2.4n MeC_6H_5$ (ca. 17 % void). Contact surface map with probe radius = 1.2 Å.

packed with close F…F contacts and face-to-face π-stacking between the coordinated pyridine ring containing N4 in one sheet and the pyridine ring containing coordinated N3vi (symmetry code vi = x, $^1/_2{-}y$, $^1/_2+z$) in the adjacent sheet (centroid…centroid distance = 3.56 Å and the angle between the ring planes = 8.8°). The packing efficiency is such that the void space is only 3.4 % (calculated in Mercury 2021.3.0 [24] using a contact surface map with probe radius = 1.2 Å). and comprising small cavities and no channels.

3.7. Structure of $[Cu_2(hfacac)_4(\mathbf{2})_2]_n{\cdot}1.5n CHCl_3{\cdot}4n MeOH$

Reactions between ligand **2** and $[Cu(hfacac)_2]{\cdot}H_2O$ using MeOH and $CHCl_3$ as solvents (Table 1) led to single crystals of $[Cu_2(hfacac)_4(\mathbf{2})]_n{\cdot}1.2n CHCl_3$ (see Section 3.3) or $[Cu_2(hfacac)_4(\mathbf{2})_2]_n{\cdot}1.5n CHCl_3{\cdot}4n MeOH$. The crystallization conditions, including solution concentrations, were essentially the same and PXRD measurements were consistent with the single crystal structure of $[Cu_2(hfacac)_4(\mathbf{2})_2]_n{\cdot}1.5n CHCl_3{\cdot}4n MeOH$ being representative of the bulk material (Fig. S81). However, a comparison of the predicted PXRD from the single crystal structure of $[Cu_2(hfacac)_4(\mathbf{2})]_n{\cdot}1.2n CHCl_3$ with the PXRD of the bulk material from the crystallization tube (Fig. S82) was consistent with the presence of another component. Note that the PXRD

Table 4
Summary of TGA experiments to confirm solvent added to two of the crystal structures when a solvent mask was applied.

Compound	Initial mass of TGA sample/mg	Weight loss/mg	Weight loss/%	Calculated solvent molecules per $\{Cu_2(hfacac)_4(L)\}$
$[Cu_2(hfacac)_4(\mathbf{4})]_n \cdot 3.5n C_6H_4Cl_2$	0.90	0.19	21.1	3.0 $C_6H_4Cl_2$
$[Cu_2(hfacac)_4(\mathbf{6})]_n \cdot 2.4n MeC_6H_5$	1.95	0.22	11.3	2.3 MeC_6H_5

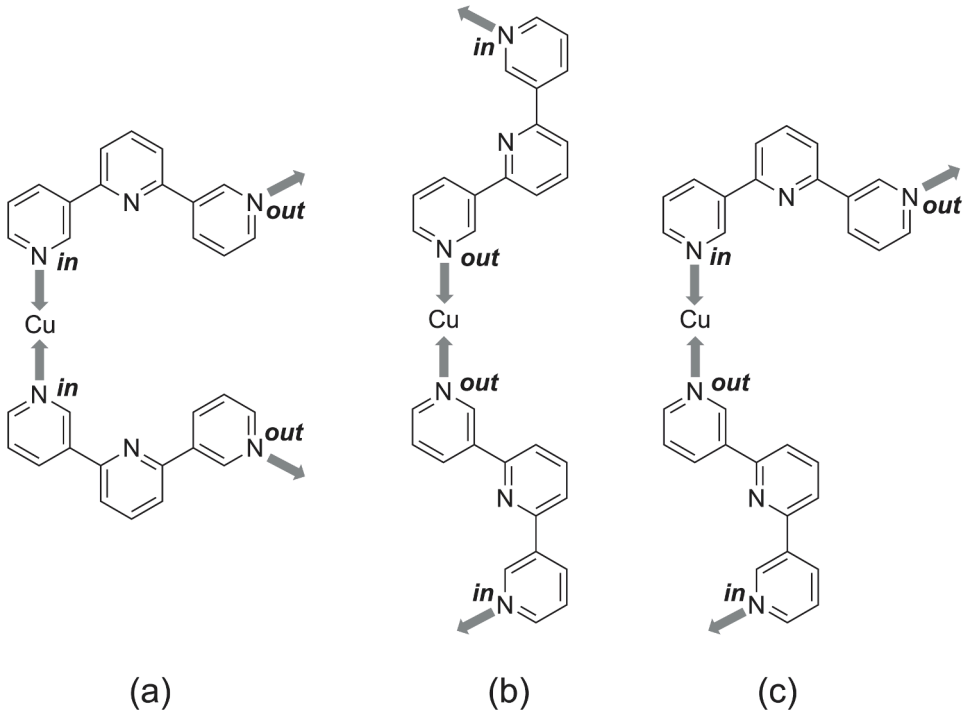

Scheme 5. Possible coordination modes (a)–(c) for the *trans*-arrangement of 3,2′:6′,3″-tpy units at a Cu centre that does not lie on an inversion centre. Limiting conformations are shown.

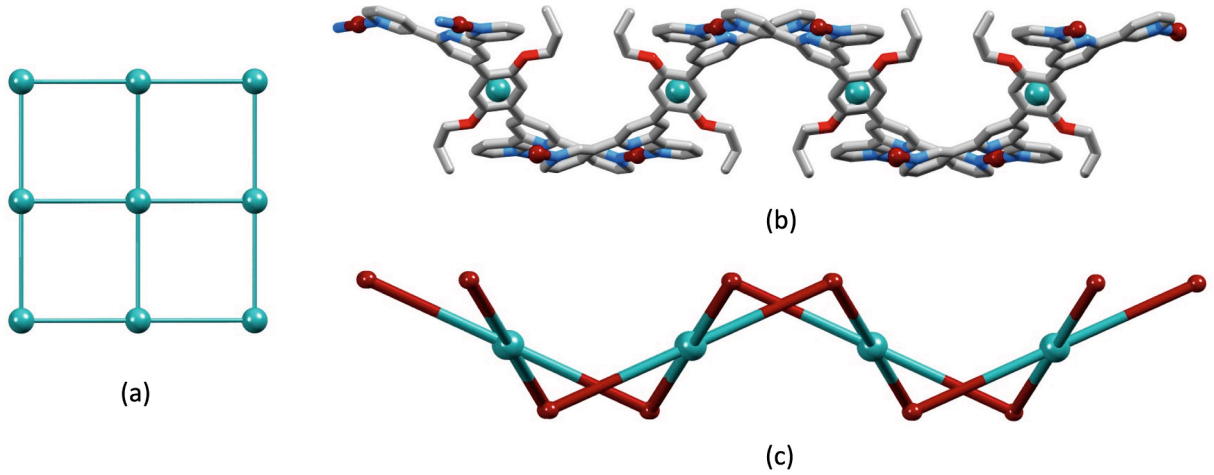

Fig. 8. (a) Part of the (4,4) net in $[Cu_2(hfacac)_4(\mathbf{3})]_n \cdot 5.5n C_6H_5Cl$; the 4-connecting node is the centroid of the arene ring in **3**. (b) View down the *c*-axis of one sheet of $[Cu_2(hfacac)_4(\mathbf{3})]_n \cdot 5.5n C_6H_5Cl$ (no H atoms, $[hfacac]^-$ ligands or solvent molecules shown); the ligand nodes are shown as turquoise spheres. (c) The same view as in (b) showing only the Cu atoms and ligand nodes.

and single XRD data were collected at 298 and 150 K, respectively.

$[Cu_2(hfacac)_4(\mathbf{2})_2]_n \cdot 1.5n CHCl_3 \cdot 4n MeOH$ crystallizes in the orthorhombic space group $Pca2_1$, and the asymmetric unit which contains a complete ligand **2** is shown in Fig. S83; atom numbering is given in the figure caption to Fig. S83. Each 3,2′:6′,3″-tpy unit adopts conformation **II** (Scheme 1 and Fig. 11a). The angles between the pyridine rings in each 3,2′:6′,3″-tpy domain are similar (31.1 and 32.0° for the unit with N1, N2, N3 compared to 20.4 and 31.9° for that with N4, N5, N6); the angles between the pyridine ring with N2 or N5 and the central arene ring of **2** are also similar (33.9 and 31.7°). Ligand **2** coordinates to two

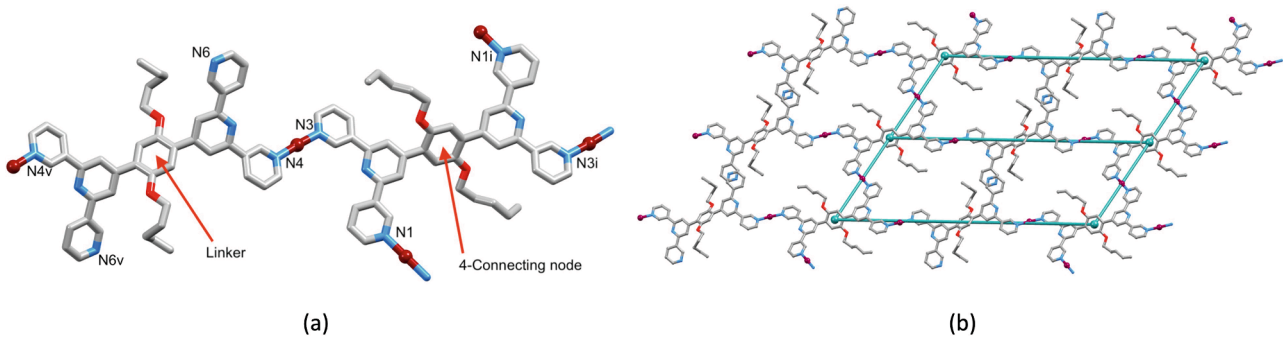

Fig. 9. The assembly in $[Cu_3(hfacac)_6(\mathbf{5})_2]_n$: (a) the two topologically different ligands **5** (symmetry codes: i = –*x*, 1–*y*, –*z*; iii = 1–*x*, –*y*, 1–*z*, consistent with Fig. S80), and (b) part of the (4,4) net with the ligand nodes depicted as turquoise spheres.

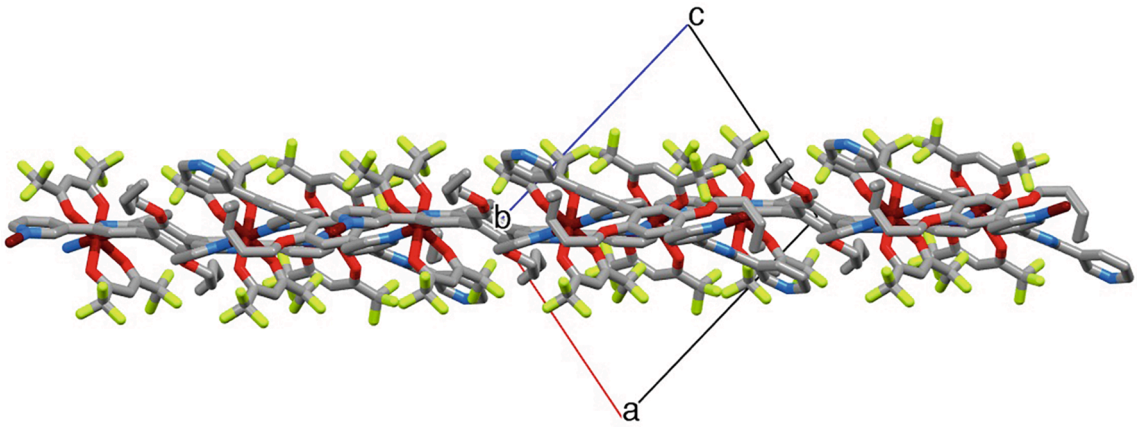

Fig. 10. Part of one sheet in $[Cu_3(hfacac)_6(\mathbf{5})_2]_n$, viewed down the *b*-axis (H atoms omitted).

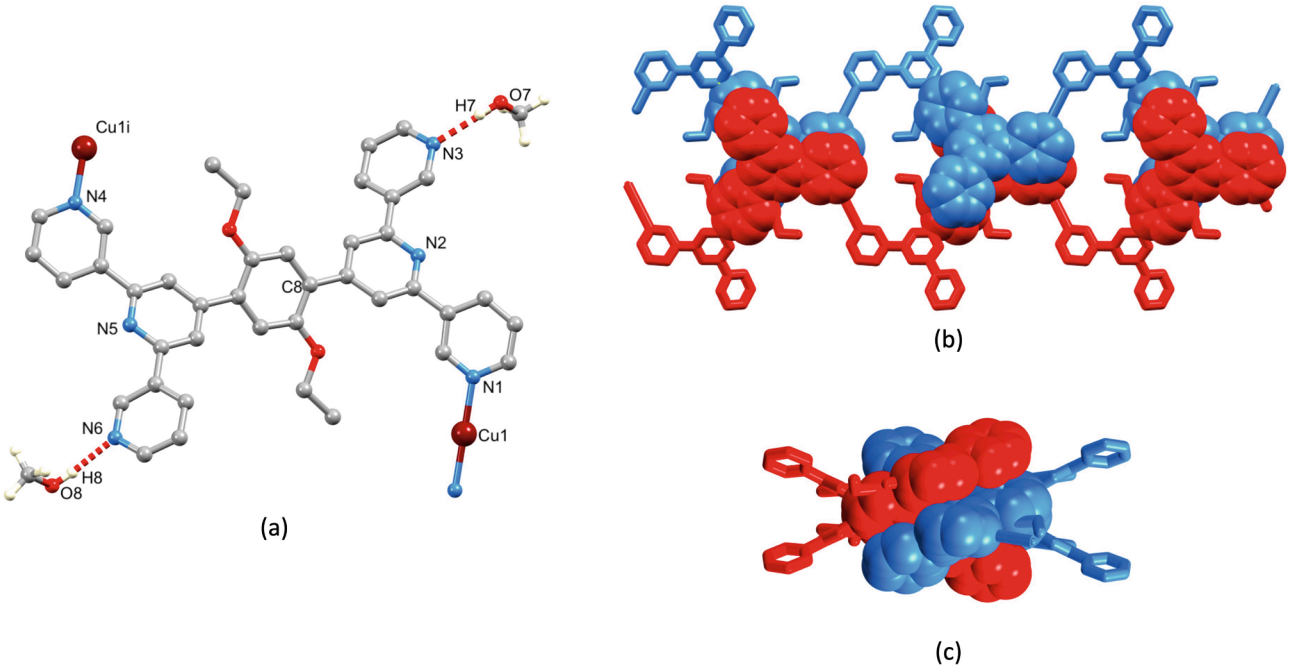

Fig. 11. (a) Repeat unit in $[Cu_2(hfacac)_4(\mathbf{2})_2]_n{\cdot}1.5n CHCl_3{\cdot}4n MeOH$ showing hydrogen-bonded MeOH molecules. Face-to-face π-interactions between $[Cu_2(hfacac)_4(\mathbf{2})_2]_n$ 1D-chains viewed (b) down the *b*-axis and (c) down the *a*-axis.

{Cu(hfacac)$_2$} units through atoms N1 and N4, while N3 and N6 in the remaining two outer pyridine rings form hydrogen bonds to MeOH solvent molecules (Fig. 11a); hydrogen bond metrics are N3…O7 = 2.780(8) Å, N6…O8 = 2.788(8) Å, N3…H7–O7 = 168.7°, N6…H8–O8 = 168.7°. The hydrogen-bonded MeOH molecules account for half of the MeOH molecules in the structure; the remainder are accommodated in channels (see Section 3.7). The copper(II) centre is in a six-coordinate environment with a *trans*-arrangement of ligands **2** (Fig. 11a). The Cu–O and Cu–N bond lengths are unexceptional (Cu–N = 1.999(5) and 2.009(5) Å, Cu–O = 2.066(4), 2.196(5), 2.212(5), 2.050(4) Å). [Cu$_2$(hfacac)$_4$(**2**)$_2$]$_n$ 1D-polymer chains follow the crystallographic *a*-axis, and adjacent chains are threaded over one another, engaging in face-to-face π-interactions between tpy-arene units as shown in Fig. 11b and 11c. The stacking interactions are consistent with the comparable twist angles between aromatic rings in the independent 3,2′:6′,3″-tpy units (see above). Centroid…centroid distances for pairs of stacked rings containing N4/N1^{ii} = 3.88 Å, N5/N2^{ii} = 3.78 Å, C8/N3^{ii} = 3.64 Å, N6/C8^{ii} = 3.63 Å (symmetry code ii = $^1/_2$–*x*, *y*, $-^1/_2 + z$); the corresponding angles between the planes of pairs of these stacked rings are 11.6, 4.1, 2.3 and 2.9°.

3.8. Thermogravimetric (TGA) investigations

We selected the 1D-polymer [Cu$_2$(hfacac)$_4$(**2**)$_2$]$_n$·1.5*n*CHCl$_3$·4*n*MeOH for TGA analysis since PXRD confirmed the composition of the bulk sample, and no solvent mask was used to treat the solvent region. Fig. 12 shows a representation of part of the crystal lattice in which all solvent molecules except the hydrogen-bonded MeOH are omitted. Large channels follow the *c*-axis, accounting for ca. 42 % void space (calculated in Mercury 2021.3.0 [24] using a contact surface map with probe radius = 1.2 Å).

First, TGA measurements coupled with mass spectrometric detection were used to investigate removal of solvent from the crystal lattice of crystals of [Cu$_2$(hfacac)$_4$(**2**)$_2$]$_n$·1.5*n*CHCl$_3$·4*n*MeOH from the crystal lattice. In the first cycle (Table 5), crystals were heated to 170 °C and loss of both MeOH and CHCl$_3$ was detected with mass peaks at *m/z* 31.0 (arising from CH_3O^+) and *m/z* 83.0 and 85.0 (arising from $CH^{35}Cl_2^+$ and $CH^{35}Cl^{37}Cl^+$) respectively (Fig. 13a). A weight loss of 14.2 % corresponded to 4.8 molecules of MeOH and 1.8 molecules of chloroform per formula unit. The number of solvent molecules is higher than reported in the formula in the single crystal structure, but is probably within experimental error. During this first cycle, the sample retained its crystallinity, which is consistent with a robust framework established by the threading of the 1D-coordination polymer chains (Figs. 11 and 12). We were therefore motivated to investigate the ability of the coordination network to re-absorb solvent molecules.

The same sample obtained after the first cycle was exposed to a mixture of CD$_3$OD and CDCl$_3$ vapour (solvent ratio 1:1, 99.8 atom % D for both solvents) for 24 h and was again analysed using TGA. Deuterated solvents were used in order to unambiguously demonstrate re-entry of solvent molecules. Loss of CDCl$_3$ and CD$_3$OD was confirmed by the presence of mass peaks at *m/z* 84.0 and 86.0 ($C^2H^{35}Cl_2^+$ and $C^2H^{35}Cl^{37}Cl^+$) and *m/z* 33.0 (CD_2HO^+) (Fig. 13b). The weight loss of 11.9 % (Table 5) was consistent with two molecules of CDCl$_3$ and one CD$_2$HOD per formula unit. Finally, a TGA measurement was carried out to examine whether MeOH could be replaced by EtOH. The resulting sample after the second cycle TGA was exposed to EtOH vapour for 24 h. The subsequent TGA/MS analysis showed only a small loss of H$_2$O (mass loss of 0.06 mg, accuracy limit of the used crucibles) but no loss of EtOH, consistent with no uptake of EtOH in the crystal lattice.

Table 5
Results of the TGA investigation of loss and re-entry of lattice solvent in [Cu$_2$(hfacac)$_4$(**2**)$_2$]$_n$·1.5*n*CHCl$_3$·4*n*MeOH.

Cycle	Initial mass/mg	Weight loss/mg	Weight loss/%	Calculated solvent molecules per formula unit
1st cycle	2.11	0.30	14.2	4.8 MeOH; 1.8 $CHCl_3$
2nd cycle	1.59[a]	0.19	11.9	1.0 CD_3OD; 2.0 $CDCl_3$
3rd cycle	1.22[a]	0.06	4.9	–

[a] The starting mass in the 2nd cycle is less than the final mass in the 1st cycle because the sample was transferred to a new crucible in the TGA instrument; similarly for the 2nd and 3rd cycles.

4. Conclusions

We have described the syntheses and characterization of seven 1,4-bis(*n*-alkyloxy)-2,5-bis(3,2′:6′,3′′-terpyridin-4′-yl)benzene ligands **1–7** and have investigated the reactions between ligands **1–8** with [Cu(hfacac)$_2$]·H$_2$O under conditions of crystal growth by layering at room temperature using different combinations of solvents. The single crystal structures of a series of coordination 2D-networks and one 1D-polymer were determined, showing that the bis(3,2′:6′,3′′-tpy) ligands typically function as 4-connecting nodes, binding four {Cu(hfacac)$_2$} units, either with the 3,2′:6′,3′′-tpy unit adopting conformation **I** or **II** (Scheme 1). However, the bis(3,2′:6′,3′′-tpy) may also serve as a 2-connecting linker. The coordination assemblies fall into four classes. The most prevalent class [Cu$_2$(hfacac)$_4$(L)]$_n$·*n*Solv (L = **1**, **4–8**; Solv = solvent, see Table 3) comprises (4,4) nets with the Cu atoms residing in the plane defined by the ligand nodes. Despite the differing lengths of the alkyloxy chains, the (4,4) net remains a robust motif; with the exception of the OEt substituents, the alkyloxy chains are directed above and below the network and the longest chains are accommodated in cavities in an adjacent sheet. One of two assemblies isolated in different experiments with

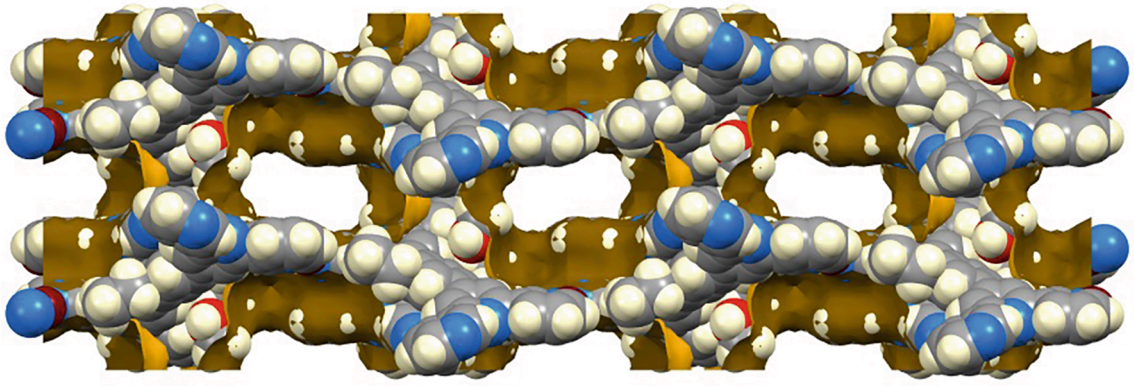

Fig. 12. Representation of the solvent-accessible void space in the crystal lattice of [Cu$_2$(hfacac)$_4$(**2**)$_2$]$_n$·1.5*n*CHCl$_3$·4*n*MeOH viewed down the *c*-axis (contact surface map with probe radius = 1.2 Å); all solvent molecules except the hydrogen-bonded MeOH are omitted.

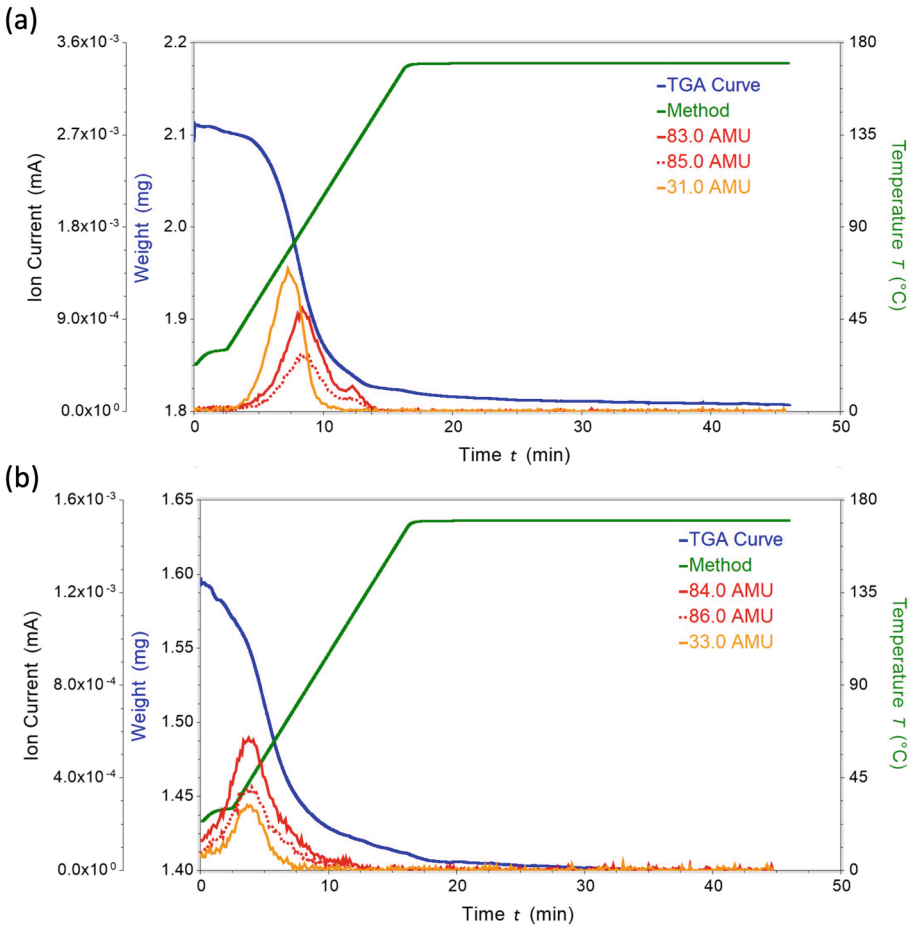

Fig. 13. TGA and mass spectrometric traces for the analysis of $[Cu_2(hfacac)_4(\mathbf{2})_2]_n{\cdot}1.5n CHCl_3{\cdot}4n MeOH$: (a) first cycle, (b) second cycle (see text). Green trace: temperature vs time; blue trace: weight of sample vs time; red and orange traces: mass detection for stated *m/z* values. See Table 5 for details of sample weights. ((Colour online.))

ligand **2** is also a (4,4) net, but PXRD revealed that this was not representative of the bulk material. The second assembly with **2** was $[Cu_2(hfacac)_4(\mathbf{2})_2]_n{\cdot}1.5n CHCl_3{\cdot}4n MeOH$, a 1D-coordination polymer in which all the bis(3,2′:6′,3′′-tpy) ligands are 2-connecting linkers; PXRD confirmed that this structure was representative of the bulk material. $[Cu_2(hfacac)_4(\mathbf{3})]_n{\cdot}5.5n C_6H_5Cl$ is unique in assembling a (4,4) net with the Cu(II) centres lying above and below the plane of the net. A third class of assembly was observed for $[Cu_3(hfacac)_6(\mathbf{5})_2]_n$; the structure is an unusual (4,4) net in which half of the ligands are 4-connecting nodes and half are 2-connecting linkers, and the efficient packing of layers leaves no solvent-accessible voids. Because of solvent disorder, most structural determinations employed a solvent mask, and TGA-MS measurements were used for selected compounds to confirm the identities and amounts of solvent molecules that were added to the crystallographic data.

Author contributions

Experimental: G.M. and S.S.C.; Crystallography: A.P. and G.M.; powder diffraction and analysis: G.M. and S.S.C.; manuscript writing and structure analysis: S.S.C. and C.E.H.; manuscript editing: all authors; funding, project concepts and supervision: C.E.H. and E.C.C.

Declaration of Competing Interest

The authors declare that they have no known competing financial interests or personal relationships that could have appeared to influence the work reported in this paper.

Data availability

Data will be made available on request.

Acknowledgements

We acknowledge financial support from the Swiss National Science Foundation (grant number 200020_182559) and the University of Basel.

Appendix A. Supplementary data

Supplementary data to this article can be found online at https://doi.org/10.1016/j.poly.2022.116005.

References

[1] Y.M. Klein, E.C. Constable, C.E. Housecroft, A. Prescimone, CrystEngComm 17 (2015) 2070–2073, https://doi.org/10.1039/c4ce02347a.
[2] G. Manfroni, A. Prescimone, S.R. Batten, Y.M. Klein, D.J. Gawryluk, E.C. Constable, C.E. Housecroft, Crystals 9 (2019) 529, https://doi.org/10.3390/cryst9100529.
[3] G. Manfroni, A. Prescimone, E.C. Constable, C.E. Housecroft, CrystEngComm 24 (2022) 491–503, https://doi.org/10.1039/d1ce01531a.
[4] E.C. Constable, C.E. Housecroft, J. Inorg. Organomet. Polym. Mater. 28 (2018) 414–427, https://doi.org/10.1007/s10904-017-0671-0.
[5] C.E. Housecroft, E.C. Constable, Chem. Commun. 56 (2020) 10786–10794, https://doi.org/10.1039/d0cc04477f.
[6] E.C. Constable, C.E. Housecroft, Coord. Chem. Rev. 350 (2017) 84–104, https://doi.org/10.1016/j.ccr.2017.06.006.
[7] B.-C. Wang, X.-L. Chen, H.-M. Hu, H.-L. Yao, G.-L. Xue, Inorg. Chem. Comm. 12 (2009) 856–859, https://doi.org/10.1016/j.inoche.2009.06.038.

[8] T.-H. Zhang, C. Bai, H.-M. Hu, J.-L. Zhang, X.-Y. Li, X. Wang, B.-Z. Wang, J. Solid State Chem. 298 (2021), 122148, https://doi.org/10.1016/j.jssc.2021.122148.
[9] Y.M. Klein, A. Prescimone, E.C. Constable, C.E. Housecroft, Aust. J. Chem. 70 (2017) 468–477, https://doi.org/10.1071/CH16527.
[10] J. Granifo, R. Gavino, E. Freire, R. Baggio, J. Mol. Struct. 1006 (2011) 684–691, https://doi.org/10.1016/j.molstruc.2011.10.038.
[11] T.-T. Wang, J.-L. Zhang, H.-M. Hu, Y. Cheng, L.-L. Xue, X. Wang, B.-Z. Wang, Polyhedron 151 (2018) 43–50, https://doi.org/10.1016/j.poly.2018.05.017.
[12] Y.M. Klein, A. Lanzilotto, A. Prescimone, K.W. Kramer, S. Decurtins, S.-X. Liu, E. C. Constable, C.E. Housecroft, Polyhedron 129 (2017) 71–76, https://doi.org/10.1016/j.poly.2017.03.030.
[13] Y. Cheng, M.-L. Yang, H.-M. Hu, B. Xu, X. Wang, G. Xue, J. Solid State Chem. 239 (2016) 121–130, https://doi.org/10.1016/j.jssc.2016.04.002.
[14] M. Zhao, J. Tan, J. Su, J. Zhang, S. Zhang, J. Wu, Y. Tian, Dyes Pigm. 130 (2016) 216–225, https://doi.org/10.1016/j.dyepig.2016.03.005versat.
[15] L. Zhang, C.-J. Li, J.-E. He, Y.-Y. Chen, S.-R. Zheng, J. Fan, W.-G. Zhang, J. Solid State Chem. 233 (2016) 444–454, https://doi.org/10.1016/j.jssc.2015.11.020.
[16] J. Granifo, M. Vargas, M.T. Garland, A. Ibanez, R. Gavino, R. Baggio, Inorg. Chem. Commun. 11 (2008) 1388–1391, https://doi.org/10.1016/j.inoche.2008.09.009.
[17] J. Yoshida, S. Nishikiori, H. Yuge, J. Coord. Chem. 66 (2013) 2191–2200, https://doi.org/10.1080/00958972.2013.800865.
[18] C.R. Groom, I.J. Bruno, M.P. Lightfoot, S.C. Ward, Acta Cryst. B 72 (2016) 171–179, https://doi.org/10.1107/S2052520616003954.
[19] G. Manfroni, S.S. Capomolla, A. Prescimone, E.C. Constable, C.E. Housecroft, Inorganics 9 (9) (2021) 54, https://doi.org/10.3390/inorganics9070054.
[20] L. Palatinus, G. Chapuis, J. Appl. Cryst. 40 (2007) 786–790, https://doi.org/10.1107/S0021889807029238.
[21] L. Palatinus, S.J. Prathapa, S. van Smaalen, J. Appl. Cryst. 45 (2012) 575–580, https://doi.org/10.1107/S0021889812016068.
[22] O.V. Dolomanov, L.J. Bourhis, R.J. Gildea, J.A.K. Howard, H. Puschmann, J. Appl. Cryst. 42 (2009) 339–341, https://doi.org/10.1107/S0021889808042726.
[23] G.M. Sheldrick, Acta Cryst. C 27 (2015) 3–8, https://doi.org/10.1107/S002188980600731X.
[24] C.F. Macrae, I. Sovago, S.J. Cottrell, P.T.A. Galek, P. McCabe, E. Pidcock, M. Platings, G.P. Shields, J.S. Stevens, M. Towler, P.A. Wood, J. Appl. Cryst. 53 (2020) 226–235, https://doi.org/10.1107/S1600576719014092.
[25] N. Kuhnert, A. Lopez-Periago, G.M. Rossignolo, Org. Biomol. Chem. 3 (2005) 524–537, https://doi.org/10.1039/b414747m.
[26] A. Parikh, H. Parikh, K. Parikh in *Name Reactions in Organic Synthesis* (2006) pp. 79-81, Cambridge University Press, Cambridge. doi:10.1017/UPO9788175968295.023.
[27] J. Wang, G.S. Hanan, Synlett 8 (2005) 1251–1254, https://doi.org/10.1055/s-2005-868481.